Divergence Analysis of Discrete 2-d Shapes

David Brunner and Guido Brunnett
Chemnitz University of Technology
Germany
{brunner, brunnett}@informatik.tu-chemnitz.de

ABSTRACT

In this paper we introduce a second order differential operator in order to partition discrete objects into meaningful parts. One of these parts contains all points of the object's medial axis which is a widely used shape descriptor.

Since aliasing is a fundamental problem for methods based on the boundary of discrete objects we use a bilateral filter to reduce the artefacts significantly.

As a result of the partitioning and filtering we obtain a lattice point set (a superset of the medial axis) which is robust against noise and aliasing and which is rotationally invariant. The lattice point set can be used for instance to compute the medial axis or similar shape descriptors.

Keywords: 2-d shape descriptor, bilateral filter, skeletonization, curve skeletons

1 INTRODUCTION

One typical goal for processing a discrete 2-d shape $\mathscr{S}$ is finding a good shape descriptor. One possible descriptor of $\mathscr{S}$ is the medial axis which is defined as the set of centres (and radii) of maximal disks in $\mathscr{S}$, whereas a disk is said to be maximal in $\mathscr{S}$, if it is not completely covered by any other disk in $\mathscr{S}$ (cf. [1, 12]). Such descriptors are widely used in many applications such as shape analysis, shape representation, skeletonization, segmentation, and shape matching (cf. [10, 5, 9]).

In this paper we use the divergence of a scalar distance field in order to describe the shape's local geometry. We show that only points located at the medial axis have a high negative divergence. Of course these points could be used in the computation of the medial axis as the contributions of Siddiqi et al. show (cf. [15, 2, 4]). On the other hand, points at concave boundary regions have a positive divergence and may be used in a segmentation approach.

But this property is only helpful for objects with a smooth boundary and therefore aliasing is a fundamental problem. Boundary based approaches are notoriously instable to small boundary perturbations. Hence, the results of corresponding algorithms such as for the medial axis are not rotationally invariant. Many methods follow the concept of reducing the influence of aliasing using some sort of heuristic. In the context of skeleton extraction pruning approaches are used for such a reducing effect [16, 7, 14].

In contrast to such heuristics, we suggest a significant reduction on the basis of a bilateral filter (whose theoretical foundations have been widely developed, recently). The bilateral filter has its origin in [17] and is typically used in applications such as denoising of images [19] or meshes [6]. Practically, the filter can be applied at interactive speed thanks to efficient numerical schemes [18]. A good survey of this field can be found in [11].

Since the points with a high negative divergence are of interest for a shape descriptor we utilize the bilateral filter to emphasize the respective regions. We show that the filtered point set is suitable to construct a shape descriptor which is rotationally invariant and very robust against boundary perturbations.

This paper is structured as follows: After introducing some mathematical basics and notations in section 2 we explain an adapted Laplace operator and the partitioning in section 3. In section 4 we analyse artefacts which are caused by the aliasing and describe the bilateral filter which is used to reduce these artefacts significantly. To demonstrate the qualities and effectiveness of the introduced operator and filter we present in section 5 as an exemplary application a skeletonization approach which uses the filtered point set to construct a shape descriptor. The paper is concluded with our results in section 6.

2 BASIC DEFINITIONS AND NOTATIONS

We use the Cartesian point lattice $\mathbb{Z}^2$ as the mathematical model for describing a tessellation of the 2-d Euclidean space $\mathbb{E}^2$ into cell elements. The coordinates of a lattice point $p \in \mathbb{Z}^2$ are denoted by p_x, p_y. For the

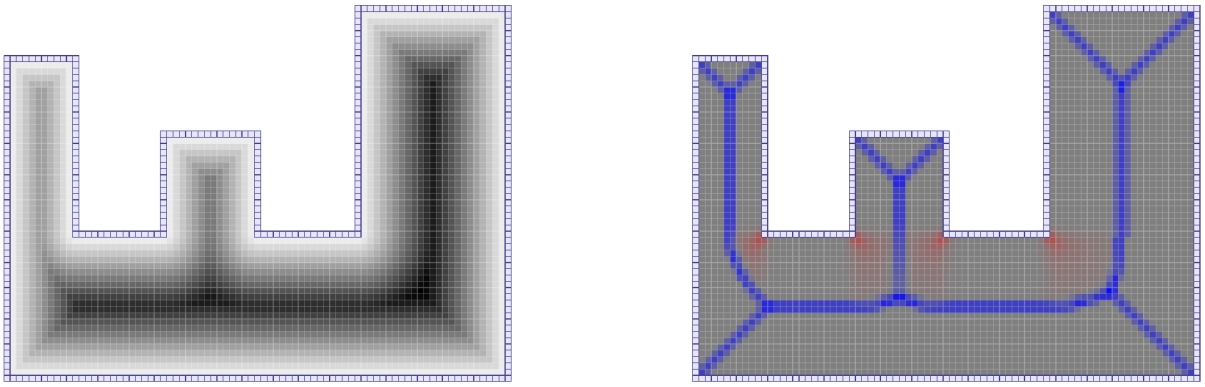

(a) (b)

Figure 1: In (a) the distance field and (b) the divergence are shown. Gray cells in (b) have zero, blue cells have a negative and red cells a positive divergence.

Cartesian lattice we define the local neighborhood of size k for lattice points by

$$N_k(p) = \left\{ q \in \mathbb{Z}^2 : \max\left(|p_x - q_x|, |p_y - q_y|\right) = k \right\} \quad (1)$$

which is based on the chessboard metric.

A discretized object O is defined as a connected finite set of lattice points $\mathbb{Z}^2$. Using the notion of a binary image it is common to say that each point of O belongs to the foreground while the points of $\overline{O} = \mathbb{Z}^2 \setminus O$ form the background.

The border of a discretized object O is defined by the set O_B of all points $p \in O$ whose local neighborhood $N_1(p)$ contains at least one point q with $q \in \overline{O}$.

3 OBJECT'S PARTITIONING

For further analysis of a discrete object O we want to partition it into three disjoint parts. The first part O_I is some kind of scaffold of the object and is similar to the medial axis. The second part O_{II} contains points which are influenced by a concave boundary. The remaining third part O_{III} is not of interest because it contains no applicable information.

Due to partition objects we start with a distance mapping. Therefore, we use a distance transform which is an efficient standard procedure to compute the minimal Euclidean distance of each object point to the background (cf. [3, 13]). Figure 1(a) shows an example.

We change this definition a little by defining the minimal Euclidean distance $d_{\min}$ of $p \in O \cup \overline{O}$ to the boundary O_B instead to the background:

$$d_{\min}(p, O_B) = \min\left(\|p,q\| : q \in O_B\right) \quad (2)$$

where $\|p,q\|$ denotes the Euclidean distance between two lattice points. We define the final distance mapping

$$d(p) = \begin{cases} -d_{\min}(p, O_B): & p \in \overline{O} \\ 0: & p \in O_B \\ d_{\min}(p, O_B): & p \in O \end{cases}. \quad (3)$$

We need to define negative distances for background points in order to make it possible to have a suitable second derivative for boundary points, too. Otherwise, all boundary points would have positive divergence and thus concave boundary would not be recognizable (since all boundary points would belong to O_{II}).

After the distance transform, we use an adapted Laplace operator to compute the divergence of distance map. The Laplace operator is a second order differential operator in $\mathbb{E}^2$ and in our case defined as the divergence of the gradient of the distance field.

The gradient of the distance field is defined to be the vector field whose components are the partial derivatives of the distance field. The gradient of a point $p = (p_x, p_y)^T \in O$ is defined by:

$$\nabla d(p) = \left(\frac{\partial d(p)}{\partial x}, \frac{\partial d(p)}{\partial y} \right)^T. \quad (4)$$

which we will compute by a finite difference since we use a discrete scalar field:

$$\nabla d(p) = \frac{1}{2} \begin{pmatrix} d((p_x+1, p_y)^T) - d((p_x-1, p_y)^T) \\ d((p_x, p_y+1)^T) - d((p_x, p_y-1)^T) \end{pmatrix}. \quad (5)$$

Finally, we compute the divergence of the vector field to measure the magnitude of the field's sink at a given point (see figure 1(b)). In general, the divergence of a differentiable vector field is defined as the sum of the partial derivatives of the i-th component:

$$\Delta d(p) = \nabla^2 d(p) = \frac{\partial^2 d(p)}{\partial x^2} + \frac{\partial^2 d(p)}{\partial y^2}. \quad (6)$$

Siddiqi et al. state in [15] that this definition cannot be used since the gradient of the distance field is not free of singularities and hence is not differentiable. Therefore, they suggest a numerically stabble solution, which we will adapt, such that $\Delta d(p) \mapsto [-1, 1]$:

$$\Delta d(p) = \frac{1}{|N_1(p)|} \sum_{q \in N_1(p)} \angle(q - p, \nabla d(q)) \quad (7)$$

where $|N_1(p)|$ is the number of local neighbor points, 8 in the 2-d case, and where $\angle \mapsto [-1,1]$ is a function which computes the cosine of angle α between two vectors $\vec{u},\vec{v}$ taking account of zero vectors:

$$\cos(\alpha) = \angle(\vec{u},\vec{v}) = \begin{cases} 0 & : \vec{u} \equiv \vec{0} \vee \vec{v} \equiv \vec{0} \\ \dfrac{\langle \vec{u},\vec{v} \rangle}{\|\vec{u}\| \, \|\vec{v}\|} & : \text{else} \end{cases} . \quad (8)$$

Now we analyse the divergence values for different point classes. Let $D(p) \subset O$ be the set of points of the maximal disc in O with p as disc center. That is, $D(p)$ describes the disc with the largest radius of all possible discs at p. Further, let

$$B(p) = D(p) \cap O_B \quad (9)$$

be the set of all border points in $D(p)$.

We are not only interested in the border points of $B(p)$. Since the divergence of a point p (defined in eq. (7)) depends on its local neighbors $N_1(p)$, the closest boundary points of those neighors are of interest, too. In order to analyse the divergence value at p we need to consider the gradients of the point set

$$\mathscr{B}(p) = \bigcup_{q \in N_1(p)} B(q). \quad (10)$$

Note that

$$B(p) \subset \bigcup_{q \in N_1(p)} B(q). \quad (11)$$

We observe for points p located at the medial axis the set $\mathscr{B}(p)$ contains points belonging to different boundary segments. For all other points p outside the medial axis $\mathscr{B}(p)$ contains only border points located at exactly one boundary segment. In figure 2 the points p_1, p_2 are and p_3, p_4 are not part of the medial axis.

Obviously, $\Delta(p)$ correlates with the gradients of the points of $\mathscr{B}(p)$. For points in $\mathscr{B}(p)$ belonging to different boundary segments, the gradients of $q \in N_1(p)$ are oriented towards p and vary strongly. Thus, $\Delta(p)$ is negative (see points p_1, p_2 in figure 2). In contrast, for points p having in $\mathscr{B}(p)$ only border points of one boundary segment, $\Delta(p)$ may be either zero for points $b \in \mathscr{B}(p)$ having the same gradient (see point p_3 in figure 2) or may be positive if the points $b \in \mathscr{B}(p)$ describe a concave boundary segment (see point p_4 in figure 2) and some of the gradients of the points $q \in N_1(p_4)$ are oriented away from p_4.

This observation is now used to classify the points into three sets so that a given object can be partioned according to the divergence values. We define (using $\dot\cup$ (instead of $\cup$) to indicate a union of disjoint sets)

$$O = O_I \,\dot\cup\, O_{II} \,\dot\cup\, O_{III}, \quad (12)$$

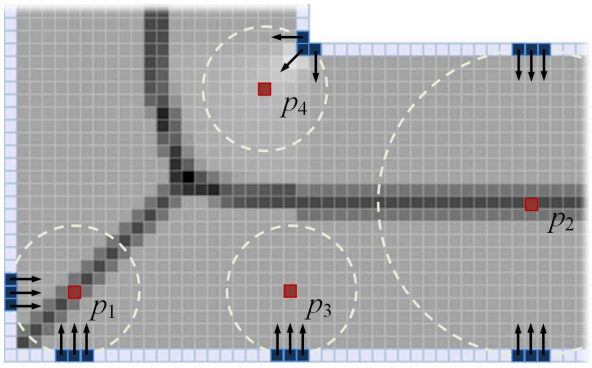

Figure 2: The divergence at different points (red) is influenced by the respective closest border points (dark blue). Dark cells representing a negative, light cells a positive divergence. The dotted circles indicate the discs $D(p_1) - D(p_4)$.

with

$$O_I = \{p : \Delta(p) < 0\}, \quad (13)$$
$$O_{II} = \{p : \Delta(p) > 0\}, \quad (14)$$
$$O_{III} = \{p : \Delta(p) = 0\}. \quad (15)$$

Fig. 1(b) illustrates the partitioning for an object with a smooth boundary (i.e. without aliasing). The blue points belong to O_I, the red points to O_{II}, and the light gray points to O_{III}.

The possible uses of these subsets of an object O are various: The set O_I contains points, which are used for example to compute the medial axis of an object. The points contained in O_{II} may be used to support a decomposition approach, since objects are often decomposed at concave regions. The points of O_{III} can be ignored depending on the particular object analysis approach, resulting in reduced computational costs.

4 FILTERING ALIASING BASED ARTEFACTS

The object shown in figure 1 contains no aliasing based artefacts, because all border segments are axis aligned. Aliasing effects occur when the object in figure 1 is rotated or noise is added and surely when an object contains non-axis aligned edges (see figure 4). The partition of O based on eq. (12) is unclear in such cases.

Obviously, the noise or aliasing causes the appearance of stripe-shaped regions of positive or negative divergence (see figure 3(a) and 3(b)). In a first filtering step the gradient field is smoothed to reduce the effects partly. Afterwards, a second filtering step is applied to the divergence field. For both filtering steps the bilateral filter is the appropriate method for removing the mentioned artefacts. This filter technique has the advantage to smooth image data while preserving its discontinuities.

In our case we intend to smooth small gradient and divergence variances while preserving the greater variances. For this purpose we adapt the well-known bilateral filter. In 2-d the Gaussian kernel is given by

$$g_\sigma(x) = \frac{1}{2\pi\sigma^2} \exp\left(-\frac{x^2}{2\sigma^2}\right). \tag{16}$$

Using this kernel we define the bilateral filter f_{grad} for lattice points p and two parameters $\sigma_d \in \mathbb{N}$, $\sigma_\nabla \in \mathbb{R}$ by:

$$f_{\text{grad}}(p) = \frac{1}{w(p)} \sum_{q \in N_{2\sigma_d}(p)} g_{\sigma_d}(\|p-q\|) g_{\sigma_\nabla}(a(p,q)) \nabla(q) \tag{17}$$

where $N_{2\sigma_d}(p)$ is the local neighborhood at p of size $2\sigma_d$ (see eq. (1)) and $w(p)$ is a normalization factor with

$$w(p) = \sum_{q \in N_{2\sigma_d}(p)} g_{\sigma_d}(\|p-q\|) g_{\sigma_\nabla}(a(p,q)). \tag{18}$$

The function $a(p,q) \mapsto [0,1]$ together with eq. (8) is defined by

$$a(p,q) = \left(\frac{1 - \angle(\nabla(p), \nabla(q))}{2}\right) \tag{19}$$

and expresses the difference between the gradients of p and q.

The amount of filtering is influenced by the parameters σ_d and σ_∇. On the one hand σ_d influences the size of the local neighborhood at p. For instance let $\sigma_d = 1$ then $N_{2\sigma_d}(p)$ defines a 5×5-mask. On the other hand the weight g_{σ_d} has the intention to decrease the influence of distant points. The second parameter g_{σ_∇} intends to decrease the influence of p's neighboring points q with a differing gradient in comparison to $\nabla(p)$.

We denote the filtered gradient at point p with $\dot{\nabla}(p)$ and the divergence based on the filtered gradients with $\dot{\Delta}(p)$:

$$\dot{\Delta}d(p) = \frac{1}{|N_1(p)|} \sum_{q \in N_1(p)} \angle(q-p, \dot{\nabla}d(q)). \tag{20}$$

See figure 3(b) and 3(c) to comprehend the filtering effect.

After applying the bilateral filter to the gradients, the divergence variation is small for neighboring points $p,q \in O_I$ in comparison to the variance between neighboring points $p \in O_I$ and $q \in O_{III}$. With this being the case, again a bilateral filtering is suitable in order to further reduce the artefacts.

Therefore, in eq. (17) the weight g_{σ_∇} is replaced by the weight g_{σ_Δ} and we get:

$$f_{\text{div}}(p) = \frac{1}{w(p)} \sum_{q \in N_{2\sigma_d}(p)} g_{\sigma_d}(\|p-q\|) g_{\sigma_\Delta}(\dot{\Delta}(p) - \dot{\Delta}(q)) \dot{\Delta}(q) \tag{21}$$

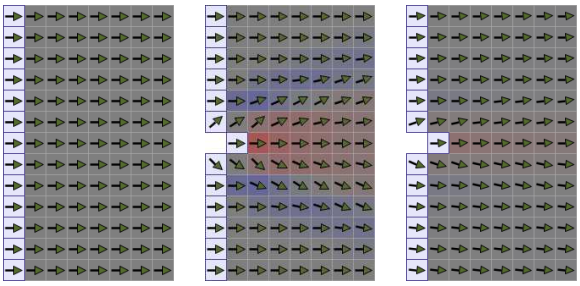

(a) (b) (c)

Figure 3: Gradient and divergences for (a) a smooth boundary, (b) with added noise, and (c) after gradient filtering.

with $w(p)$ again as the sum of all weigths. The weight g_{σ_Δ} intends to decrease the influence of p's neighboring points q with a divergence value different from $\dot{\Delta}(p)$.

We denote the filtered divergence value at point p with $\ddot{\Delta}(p)$ and redefine the decomposition of O according to the filtered divergence field:

$$O = \ddot{O}_I \cup \ddot{O}_{II} \cup \ddot{O}_{III}, \tag{22}$$

with

$$\ddot{O}_I = \left\{p : \ddot{\Delta}(p) < 0\right\}, \tag{23}$$

$$\ddot{O}_{II} = \left\{p : \ddot{\Delta}(p) > 0\right\}, \tag{24}$$

$$\ddot{O}_{III} = \left\{p : \ddot{\Delta}(p) = 0\right\}. \tag{25}$$

Note, that filtering the distance map itself wouldn not be suitable, since the variances of the distance values are only marginal and significant features would not preserved.

5 SAMPLE APPLICATION

In this chapter we present a skeletonization approach on the basis of the findings of the previous chapters in order to evaluate our shape descriptor. Therefore we use a thinning method which offers two important advantages. It is fast and furthermore the only known method where the topological equivalence of the skeleton with the initial discretized object can be guaranteed [8] (the definition of topological equivalence is based on the same number of connected components, tunnels, and cavities). Thinning algorithms iteratively remove border points (i.e. points with at least one neighbor point belonging to the background) from a discretized object. It is common to call a removable point *simple* if its removal does not change the topology of the discretized object ([8]).

We extend the standard thinning algorithm by using the filtered divergence values. This is done firstly, by sorting the removable points according to the filtered divergence values, such that points with high positive divergence are prioritized and points with high negative

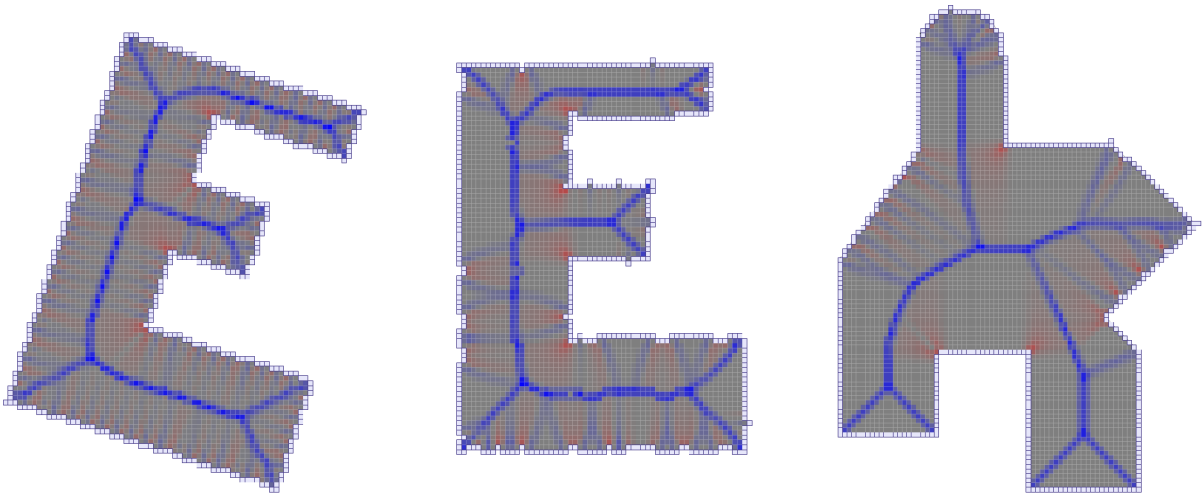

(a) (b) (c)

Figure 4: For non-axis aligned boundary segments aliasing based artefacts occur.

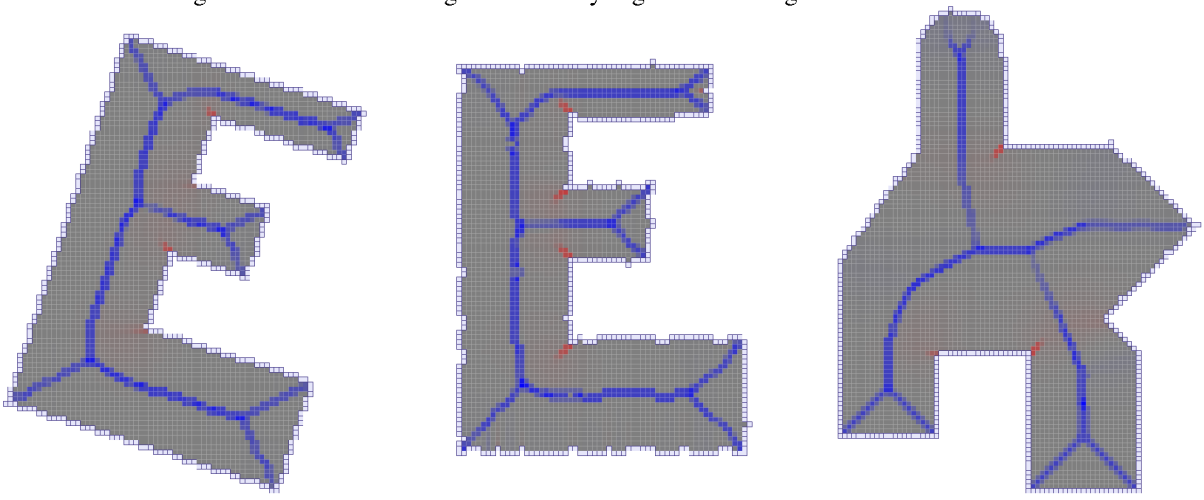

(a) (b) (c)

Figure 5: Filtering results for $\sigma_d = 2$, $\sigma_\nabla = 0.05$, and $\sigma_\Delta = 0.01$ are shown.

divergence are considered at last (as suggested in [4]). Secondly, a divergence-based threshold t is used to prevent the removal of points with a high negative divergence. The resulting algorithm is structured as follows:

```
do {
   something changed = false;
   bp = determine all border points;
   sort bp; // desc. divergence values

   for each p in bp {
      if (p is simple) and (Δ̈(p) ≥ t) {
         remove p
         something changed = true;
      }
   }
} while something changed
```

After applying the sketched algorithm the resulting skeletons are not necessarily thin. The thinning algorithm is once again applied to the remaining point set with changed conditions. The threshold-based condition is replaced by the curve-end-point-condition, which states that a point with only one foreground-neighbor must not be removed:

```
do {
   ⋮
   for each p in bp {
      if (p is simple) and (|N1(p)| > 1) {
         remove p
         something changed = true;
      }
   }
} while something changed
```

Sorting the border points by divergence changes the order of point removal. By removing a point p the removability of its neighbors may be changed. That is, a point q may not be removed only because its neighbor (which has a higher divergence) p is removed before considering q.

The resulting skeletons provide very positive properties: they are efficient to compute, topological equivalent to the original object, centered, rotationally invariant, and robust against noise (see figure 6). Furthermore, the divergence-based threshold t allows the generation of hierarchical skeletons – which is a very rare possibility with regard to the wide range of available skeletonization methods. See figure 7 for a sample.

6 RESULTS AND CONCLUSION

It is clearly recognizable that bilateral filtering of the divergence values reduces the aliasing based artefacts substantially. As a beneficial consequence, the point set $\ddot{O}_I$ is rotationally invariant and robust against noise. For this reason, operators or algorithms (such as skeletonization) which base on this point set, yield results with these properties. In the case of the medial axis based on the filtered point set $\ddot{O}_I$ we get a robust skeleton for noisy and rotated 2-d objects.

Another observation could be interesting for shape decomposition: Repeated filtering of the divergence values diverges quickly. The resulting connected sets of points $\in \ddot{O}_I$ are representatives for all major parts of the whole shape (see figure 8).

The presented approach may be easily adopted to discrete 3-d images.

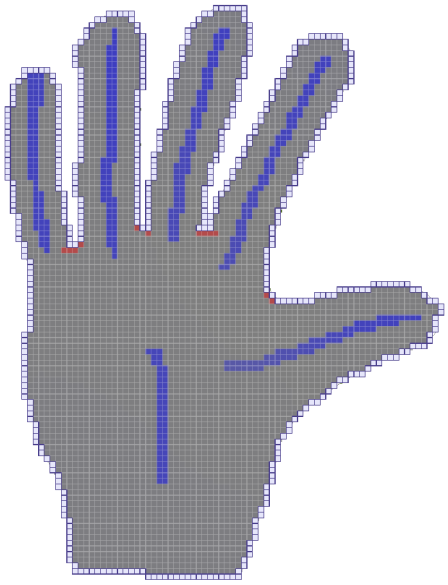

Figure 8: The set $\ddot{O}_I$ diverges if the divergence filter is repetitive applied. The resulting set may be used for a shape segmentation.

REFERENCES

[1] Harry Blum. A Transformation for Extracting New Descriptors of Shape. In Weiant Wathen-Dunn, editor, *Models for the Perception of Speech and Visual Form*, pages 362–380. MIT Press, Cambridge, 1967.

[2] Sylvain Bouix and Kaleem Siddiqi. Divergence-based medial surfaces. In *ECCV '00: Proceedings of the 6th European Conference on Computer Vision-Part I*, pages 603–618, London, UK, 2000. Springer-Verlag.

[3] Jr. Calvin R. Maurer, Rensheng Qi, and Vijay Raghavan. A linear time algorithm for computing exact euclidean distance transforms of binary images in arbitrary dimensions. *IEEE Trans. Pattern Anal. Mach. Intell.*, 25(2):265–270, 2003.

[4] Pavel Dimitrov, Carlos Phillips, and Kaleem Siddiqi. Robust and efficient skeletal graphs. *Computer Vision and Pattern Recognition, IEEE Computer Society Conference on*, 1:1417, 2000.

[5] Peter J. Giblin and Benjamin B. Kimia. On the local form and transitions of symmetry sets, medial axes, and shocks. *Int. J. Comput. Vision*, 54(1-3):143–156, 2003.

[6] Thouis R. Jones, Frédo Durand, and Mathieu Desbrun. Non-iterative, feature-preserving mesh smoothing. In *SIGGRAPH '03: ACM SIGGRAPH 2003 Papers*, pages 943–949, New York, NY, USA, 2003. ACM.

[7] Tao Ju, Matthew L. Baker, and Wah Chiu. Computing a family of skeletons of volumetric models for shape description. *Comput. Aided Des.*, 39(5):352–360, 2007.

[8] T. Yung Kong and A. Rosenfeld. Digital topology: introduction and survey. *Comput. Vision Graph. Image Process.*, 48(3):357–393, 1989.

[9] Arjan Kuijper, Ole Fogh Olsen, Philip Bille, and Peter Giblin. Matching 2d shapes using their symmetry sets. In *ICPR '06: Proceedings of the 18th International Conference on Pattern Recognition*, pages 179–182, Washington, DC, USA, 2006. IEEE Computer Society.

[10] Frederic F. Leymarie and Benjamin B. Kimia. The shock scaffold for representing 3d shape. In *In Proc. of 4th International Workshop on Visual Form (IWVF4*, pages 216–229. Springer-Verlag, 2001.

[11] Sylvain Paris, Pierre Kornprobst, Jack Tumblin, and Frédo Durand. A gentle introduction to bilateral filtering and its applications. In *SIGGRAPH '07: ACM SIGGRAPH 2007 courses*, page 3, New York, NY, USA, 2007. ACM.

[12] John L. Pfaltz and Azriel Rosenfeld. Computer representation of planar regions by their skeletons. *Commun. ACM*, 10(2):119–122, 1967.

[13] E. Remy and E. Thiel. Exact medial axis with euclidean distance. *Image and Vision Computing*, 23(2):167–175, February 2005.

[14] Dennie Reniers and Alexandru Telea. Segmenting simplified surface skeletons. *Discrete Geometry for Computer Imagery*, 4992/2008(1-3):262–274, 2008.

[15] Kaleem Siddiqi, Sylvain Bouix, Allen Tannenbaum, and Steven W. Zucker. The hamilton-jacobi skeleton. In *ICCV '99: Proceedings of the International Conference on Computer Vision-Volume 2*, page 828, Washington, DC, USA, 1999. IEEE Computer Society.

[16] Stina Svensson and Gabriella Sanniti di Baja. Simplifying curve skeletons in volume images. *Comput. Vis. Image Underst.*, 90(3):242–257, 2003.

[17] C. Tomasi and R. Manduchi. Bilateral filtering for gray and color images. In *ICCV '98: Proceedings of the Sixth International Conference on Computer Vision*, page 839, Washington, DC, USA, 1998. IEEE Computer Society.

[18] Ben Weiss. Fast median and bilateral filtering. *ACM Trans.*

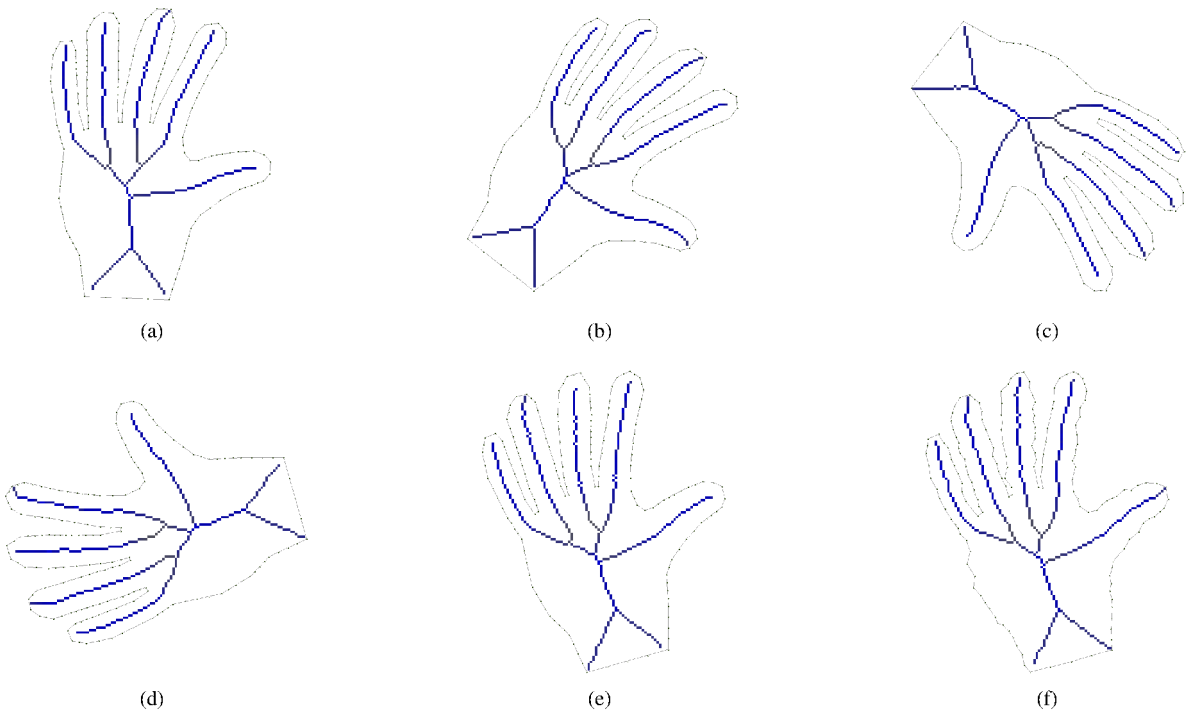

Figure 6: The contour is rotated in (a)-(e) and noise is added in (f). The resulting skeletons are nearly identically except for almost unnoticeable deviations.

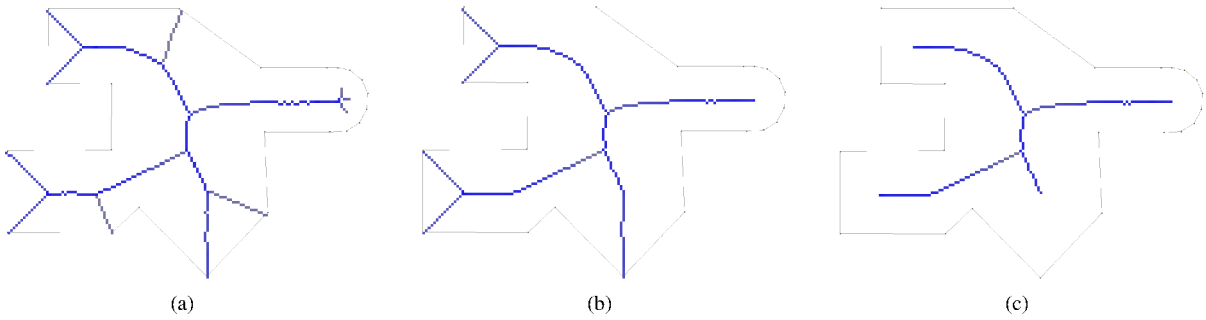

Figure 7: A hierarchical skeleton may be constructed using different thresholds. For the skeletons in (a) all points p with $\ddot{\Delta}(p) \leq -0.1$, in (b) with $\ddot{\Delta}(p) \leq -0.3$, and in (c) with $\ddot{\Delta}(p) \leq -0.5$ are preserved.

Graph., 25(3):519–526, 2006.

[19] Buyue Zhang and Jan P. Allebach. Adaptive bilateral filter for sharpness enhancement and noise removal. *IEEE Transactions on Image Processing*, 17(5):664–678, 2008.